

# **Finite Volume Time Domain Solutions of Maxwell's Equations**

**AE 397 B.Tech. Seminar**

By

**Debojyoti Ghosh  
01D01010**

Under the guidance of

**Prof. Avijit Chatterjee**

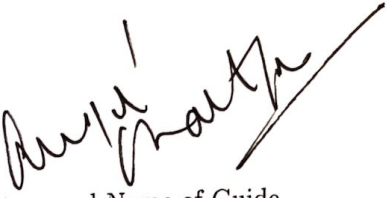


**Department of Aerospace Engineering,  
Indian Institute of Technology, Bombay  
March, 2004**

# Certificate

Certified that this B.Tech. Seminar Report titled "**Finite Volume Time Domain Solutions of Maxwell's Equations**" by Debojyoti Ghosh (01D01010) is approved by me for submission. Certified further that, to the best of my knowledge, the report represents a study work carried out by the student.

Date: 12-03-04



Signature and Name of Guide



A. Chatterjee

# Abstract

The lack of analytical solutions to the Maxwell's equations for complex configurations and situations has led to the development of numerical solutions to the Maxwell's equations. One of these involve the application of schemes developed by the CFD community to solve the Euler equations to problems in electromagnetics. The mathematically similar nature of Maxwell's equations and the unsteady Euler equations has made this possible. Problems involving complicated geometries have resulted in the development of the finite volume time domain (FVTD) framework. A study has been made of the existing FVTD schemes, including high resolution schemes. The various forms of Maxwell's equations describing wave propagation through different types of media have been studied along with the schemes applied to solve these equations. An analysis has been made of the characteristic based algorithms which are particularly attractive for solving hyperbolic problems. Numerical implementations of the physical boundary conditions have also been discussed.

*Keywords:* Computational Electromagnetics, Finite Volume method, RCS computations, Characteristic-based algorithms

# Contents

<b>1</b>	<b>Introduction</b>	<b>1</b>
<b>2</b>	<b>The Finite Volume Time Domain (FVTD) Framework</b>	<b>3</b>
2.1	Hyperbolic Conservation Laws . . . . .	3
2.2	Finite Volume Formulation . . . . .	4
2.3	Reconstruction-Evolution Schemes . . . . .	5
2.3.1	Spatial Reconstruction . . . . .	6
2.3.2	Time Evolution . . . . .	8
<b>3</b>	<b>Maxwell's Equations</b>	<b>9</b>
3.1	Differential form . . . . .	9
3.2	Integral Form . . . . .	10
3.3	Time Harmonic Fields and Wave Equation . . . . .	11
3.4	Boundary Conditions . . . . .	11
3.4.1	Finite Conductivity Media . . . . .	12
3.4.2	Infinite Conductivity Media . . . . .	12
3.5	Material Properties and Constitutive Relations . . . . .	13
3.5.1	Lossy Media . . . . .	13
3.5.2	Non-Lossy Media . . . . .	15
<b>4</b>	<b>Numerical Formulation and Solutions</b>	<b>16</b>
4.1	Characteristic based algorithms . . . . .	17
4.2	Dual Grid approach . . . . .	18
4.3	Numerical Boundary Treatment . . . . .	18
4.3.1	Surface Boundary Conditions . . . . .	18
4.3.2	Far Field . . . . .	19
4.4	An Application: RCS Computations . . . . .	20
<b>5</b>	<b>Conclusions</b>	<b>24</b>

# List of Figures

4.1	Surface currents (cylinder)	21
4.2	Computed $H_z$ for a cruciform missile at 72 MHz	21
4.3	RCS of a sphere	22
4.4	RCS of a Cone-sphere	22
4.5	RCS of an ogive	22
4.6	RCS of a NASA almond	22
4.7	RCS for a clean delta wing	23

# Nomenclature

- **A, B, C** - Flux Jacobian matrices in the Cartesian coordinate directions
- **B** - magnetic flux density
- **D** - electric flux density
- **E** - electric field intensity
- **H** - magnetic field intensity
- **F** - flux tensor
- **f, g, h** - flux vectors in Cartesian coordinate directions
- **J<sub>i</sub>** - Impressed current density
- **J<sub>c</sub>** - Conduction current density
- **J** - Total current density
- **j** - imaginary unit, square root of -1
- **k** - incident electromagnetic wave number
- **$\hat{i}, \hat{j}, \hat{k}$**  - unit vectors along Cartesian directions
- **$\hat{n}$**  - unit surface normal
- **s** - source term
- **t** - time
- **u** - state vector
- **x, y, z** - Cartesian coordinates
- **$\Omega$**  - numerical domain /sub-domain
- **$\Lambda$**  - diagonal matrix

- $\beta$  - wave coefficient
- $\epsilon$  - electric permittivity
- $\mu$  - magnetic permeability
- $\lambda$  - wavelength
- $\sigma$  - Radar Cross-Section (RCS)
- $\rho$  - volume charge density or equivalent magnetic resistivity
- $\sigma$  - electrical conductivity
- $\omega$  - angular frequency or characteristic variable
- $\chi_e$  - electric susceptibility
- $\chi_m$  - magnetic susceptibility

# Chapter 1

## Introduction

The Maxwell's Equations form the set of basic governing partial differential equations for any problem in electromagnetism and represent a fundamental unification of the electric and magnetic fields. However, analytical solutions can be found only for very elementary geometries. Closed form solutions for practical cases involve decomposing the given problem into elementary ones, either exactly or approximately, and superposing the analytical solutions of these elementary problems to get a solution to the original problem. The drawbacks of such methods are obvious. This is the prime motivation for seeking numerical solutions and has given rise to Computational Electromagnetics (CEM). One of the approaches used in CEM is the Method of Moments (MM) which involve solving frequency domain integral equations. Limitations of such approaches, for example, difficulty in including material properties, have given an impetus to seeking direct time-domain solutions to the Maxwell's equations.

Computation of time-domain solutions was first proposed by Yee in 1966[1, 2, 4]. This was a finite difference formulation, with second order spatial and temporal accuracy, on a staggered grid. This was followed by a number of finite difference time domain (FDTD) schemes with higher accuracy, resolution and better stability properties. However, to handle increasingly complicated geometries, the finite volume framework was introduced . The equations, in their conservative form, are the basis for the finite volume time domain (FVTD) formulation.

The Maxwell's equations, in the time-domain, constitute a hyperbolic problem with real eigenvalues in all spatial directions. This yields a domain of influence and a domain of dependence for each point in space, each bounded by characteristics[3]. The solution consists of information propagating along the corresponding characteristics. This property makes characteristic based algorithms particularly attractive. The advantages include ensuring the well-posedness of a problem and suppression of spurious waves generated at the truncated boundary, as discussed in later chapters. The nature of the Maxwell's equations has made it possible to apply finite volume schemes, developed to solve the Euler equations of gasdynamics, to problems in electromagnetics.

Presently, the FVTD framework suffers from the requirement of large computing resources. Solutions for realistic problems involves a huge memory as well as fast processor speeds, often

on a parallel platform. There has been a tremendous increase in the available computational power available in the past few decades, thus shortening the computation time required drastically. Algorithms developed in the recent past utilize both data parallel and message passing paradigms. Issues related to parallel algorithms have been excluded from this report and may be found in [4].

One of the major applications of the FVTD scheme is the computation of the radar cross-section (RCS) for complex bodies, especially aircraft configurations. Methods based on geometric optics, physical optics, method of moments, etc have been found to be limited in scope. FVTD algorithms, validated on canonical shapes, have been applied to find the RCS of low-observable configurations. This framework has the advantage of being able to handle complicated geometries using a single formulation. The development of robust and efficient grid-generating softwares have reduced the time required to generate grids for aircraft, thus making the process of RCS computations relatively simpler. Recent developments include solving for scattering by radar absorbing material (RAM) coated bodies using a unified formulation [5].

## Chapter 2

# The Finite Volume Time Domain (FVT) Framework

### 2.1 Hyperbolic Conservation Laws

Various physical phenomena which are time-dependent can be mathematically modeled with a system of hyperbolic partial differential equations. These phenomena consist of wave(s) propagating through the domain at finite speeds. The solutions of these equations depend both on the spatial coordinates ( $x, y, z$ ) and time. The system of PDEs usually takes the form

$$\frac{\partial \mathbf{u}}{\partial t} + \sum_{i=1}^n \frac{\partial \mathbf{f}_i}{\partial x_i} = 0 \quad (2.1)$$

Here  $\mathbf{u}$  is a column vector having, say,  $d$  components for a system of  $d$  PDEs.  $\mathbf{x}_i, i = 1, \dots, n$  are the  $n$  spatial directions in  $\mathbf{R}^d$  and  $\mathbf{f}_i$  are the flux vectors.

The aim is to find a solution  $\mathbf{u}(\mathbf{x}, t) : \Omega \times [0, \infty) \rightarrow \mathbf{R}^d$  satisfying the initial conditions  $\mathbf{u}(\mathbf{x}, 0) = \mathbf{u}_0(\mathbf{x}), \mathbf{x} \in \Omega$  and the boundary conditions  $\mathbf{u}(\mathbf{x}, t) = \phi(\mathbf{x}), \mathbf{x} \in \partial\Omega$  as specified in the given problem. The simplest example of this is the 1D advection equation[7]  $q_t + uq_x = 0$  where  $q$  is the density of the contaminant and  $u$  is the flow velocity. This equation models the behavior of a contaminant present in very small quantities in a 1D flow. It admits solutions of the form  $q(x, t) = \tilde{q}(x - ut)$ . The waveform  $\tilde{q}$  propagates with flow velocity  $u$  and unchanged shape.

Consider equation (2.1) with  $n=1$  (1-dimensional)

$$\frac{\partial \mathbf{u}}{\partial t} + \frac{\partial \mathbf{f}}{\partial x} = 0 \quad (2.2)$$

$\mathbf{f}$  is a function of  $\mathbf{u}$  and hence the equation can be written as  $\mathbf{u}_t + \mathbf{f}(\mathbf{u})_x = 0$  which is the differential form. In integral form, we get

$$\int_{x_1}^{x_2} \mathbf{u}(x, t) dx + \int_{t_1}^{t_2} f(\mathbf{u}(x_2, t)) - f(\mathbf{u}(x_1, t)) dt = 0 \quad (2.3)$$

These are the *conservative forms* since the total of the variable  $\mathbf{u}$  is being conserved. In the domain  $[x_1, x_2]$ , the value of  $\int \mathbf{u} dx$  can change only due to the flux  $f(\mathbf{u})$  at the boundaries. The differential form or the *point form* holds only if  $\mathbf{u}$  and  $f(\mathbf{u})$  are sufficiently smooth for their

derivatives to exist. The integral form, also called the *weak form*, is more fundamental and represents the physics of the problem. Equation (2.2) can be written as

$$\mathbf{u}_t + A\mathbf{u}_x = 0 \quad (2.4)$$

where  $A = f'(\mathbf{u})$  is called the *Flux Jacobian matrix*. Hyperbolicity of the system dictates that  $A$  is diagonalizable with real eigenvalues, i.e., there exists a complete set of linearly independent eigenvectors [7, 8].

For a linear problem, the matrix  $A$  is a constant and is independent of the variable  $\mathbf{u}$ , for example the Maxwell's equations. The wave nature of the solution can be explained as follows. Let  $\mathbf{u}(\mathbf{x}, t) : \Omega \times [0, \infty) \rightarrow \mathbf{R}^m$  and  $\lambda_1 \leq \lambda_2 \dots \leq \lambda_m$  be the eigenvalues of  $A$  in equation (2.4). Then  $\Lambda = P^{-1}AP$  where  $\Lambda$  is the diagonal matrix with the eigenvalues on the diagonal.  $P$  is the matrix with the right-eigenvectors as its columns. From equation (2.4), we get

$$\omega_t + \Lambda \omega_x = 0; \quad \omega = P^{-1}\mathbf{u}$$

Since  $\Lambda$  is a diagonal matrix, the system decouples into  $m$  advection-type equations

$$(\omega_p)_t + \lambda_p (\omega_p)_x = 0; \quad p = 1, 2, \dots, m$$

$\omega_p$  are called the characteristic variables and are found to be constant along curves

$$x + \lambda_p t = \text{const}$$

This form of the governing equations is particularly simple and is suitable to solve Riemann problems [7, 8].

Thus we see that a hyperbolic system of  $m$  PDEs admits solutions consisting of  $m$  waves with the eigenvalues of the system as wave speeds. Since waves travel at finite speeds, each point  $(X, T)$  has a domain of dependence and a range of influence, bounded by the characteristics.

## 2.2 Finite Volume Formulation

The finite volume formulation is based on the conservation form of the system of PDEs, for example, equation (2.3). We can re-write equation (2.1) as

$$\frac{\partial \mathbf{u}}{\partial t} + \nabla \cdot \mathbf{F} = 0$$

where  $\mathbf{F} = \{\mathbf{f}_i\}$  is the flux vector. Integrating and applying Flux-Divergence Theorem over a elemental control volume  $D_i$  (the  $i$ th cell), we get

$$\int_{D_i} \frac{\partial \mathbf{u}}{\partial t} dV + \int_{\partial D_i} \mathbf{F} \cdot d\mathbf{s} = 0$$

The discretized version of the above equation is used to find the numerical solution. As an example, for a 1-D problem, the first term  $\int_{D_i} \frac{\partial \mathbf{u}}{\partial t} dV$  can be approximated over the  $i$ th cell and  $n$ th time interval as  $\frac{\mathbf{U}_i^{n+1} - \mathbf{U}_i^n}{\Delta t} \cdot \Delta x$  where  $\Delta x$  is the length of the cell  $D_i$  and  $\Delta t$  is the time step.  $\mathbf{U}_i^n$  and  $\mathbf{U}_i^{n+1}$  are the length averaged values of  $\mathbf{u}$  over the cell  $D_i$  at time  $t_n$  and  $t_{n+1}$ . The interfaces of each cell are the points  $x_{i-1/2}$  and  $x_{i+1/2}$ . Since the waves travel at finite speeds, we can assume the flux through the interface to depend only on its immediate neighbours, thus enabling us to write the numerical flux function as

$$\hat{\mathbf{g}}_{i-1/2}^n = f(\mathbf{U}_i^n, \mathbf{U}_{i-1}^n)$$

A numerical flux  $\hat{g}_{i-1/2} = f(u_{j-l}, \dots, u_{j+k})$  is said to be consistent if it reduces to the exact flux when applied to the exact solution, i.e.,  $\hat{g}(u, \dots, u) = f(u)$ . Consistency is required to guarantee that any convergent and bounded sub-sequence of the numerical solution has its limit a weak solution of the governing equation. Thus, we get a general explicit method for a 1-D problem as [7, 9]

$$\mathbf{U}_i^{n+1} = \mathbf{U}_i^n - \frac{\Delta t}{\Delta x} [\hat{\mathbf{g}}_{i+1/2}^n - \hat{\mathbf{g}}_{i-1/2}^n] \quad (2.5)$$

The CFL condition[8] dictates that the numerical domain of dependence should contain the physical domain of dependence. As an example, for a 1D problem using a scheme involving two time levels only, the time step should satisfy the condition

$$0 < \left(\frac{\Delta t}{\Delta x}\right)(\max \lambda_p) \leq 1$$

### 2.3 Reconstruction-Evolution Schemes

A number of finite volume based schemes have been developed by the CFD community to solve the hyperbolic unsteady Euler equations. These schemes are generally called as Reconstruction-Evolution schemes (also referred to as *Godunov-type* and *MUSCL-type* schemes) [8]. The solution is arrived at through an explicit time-marching, involving the following two steps at each time-level:

- Spatial Reconstruction of the function  $\mathbf{u}(x, t^n)$  from the discrete cell averaged values  $\mathbf{u}_i^n$  at the cell interfaces followed by calculation of the flux  $f(\mathbf{u}(x, t^n))$ .
- Temporal Evolution involving approximating the flux at the interface  $f(\mathbf{u}(x_{i+1/2}, t))$  in the interval  $[t^n, t^{n+1}]$ . The time averaged numerical flux can be expressed as  $\hat{\mathbf{g}}_{i+1/2}^n = \frac{1}{\Delta t} \int_{t^n}^{t^{n+1}} f(\mathbf{u}(x_{i+1/2}, t)) dt$

Once the numerical flux function is found, the solution at the next time level  $t^{n+1}$  is found from equation (2.5).

### 2.3.1 Spatial Reconstruction

As mentioned above, spatial reconstruction aims to find an approximate value of the flux at the cell interfaces given the discrete cell-averaged values of the solution  $\mathbf{u}_i^n$ . Piece-wise polynomial interpolation between the discrete values is used to find these fluxes. Oscillations are avoided at cells which do not contain discontinuities. Another advantage of piece-wise polynomials is that they can accommodate jump discontinuities at the cell interfaces. A number of schemes have been developed differing in their accuracy and resolution of discontinuities. The first such schemes had a first order accuracy, with piece-wise constant interpolation

$$u(x, t^n) = u_i^n, \quad x \in [x_{i-1/2}, x_{i+1/2}] \quad (2.6)$$

One such example is the Courant-Isaacson-Rees (CIR) scheme. These schemes were dissipative in nature. To get better spatial accuracy, higher order schemes were developed. Second order schemes used piece-wise linear interpolation, i.e,

$$u(x, t^n) = u_i^n + S_i^n(x - x_i), \quad x \in [x_{i-1/2}, x_{i+1/2}] \quad (2.7)$$

Here the slope  $S_i^n$  is the first divided difference of the function  $u$  based on the neighbouring cells. Examples of second-order schemes include the Lax-Wendroff scheme, the Beam-Warming scheme and the Fromm's method. These schemes were found to be dispersive in nature and resulted in oscillatory behavior near discontinuities.

Due to the limitations of first and second order schemes, high resolution schemes have been developed using techniques like solution averaging and slope limiting, to prevent oscillations near discontinuities. The aim of these techniques is to retain a high order of accuracy right upto the discontinuity. One such family of schemes was proposed by VanLeer and is called as the *Monotone Upwind Scheme for Scalar Conservation Laws* (MUSCL)[8]. These are 2nd order accurate schemes using equation (2.7) to construct the interpolating polynomial. The schemes differ in their choice of the slope  $S_i^n$ , which is found by applying some limiter to the actual slope. Some of the limiters developed are Minmod, Superbee, MC, etc [7, 8]. A variation of these schemes are the Harten-Osher Uniformly Non-Oscillatory schemes (UNO) which use the essentially non-oscillatory reconstruction for forming the slopes.

Another class of high resolution schemes are the Anderson-Thomas-VanLeer RE Methods. They consist of second and third order methods which use reconstruction via primitive function

(RP) [8] for reconstruction. The flux at the interface is split into left and right going fluxes based on the sign of the eigen-value

$$f_{i+1/2}^n = f(u_{i+1/2}^+) + f(u_{i+1/2}^-) \quad (2.8)$$

where  $u^-$  and  $u^+$  represent the values of the reconstructed polynomial on the left and right sides of the interface and thus are constructed using a leftward and rightward biased stencil respectively. For the second order case, these values are constructed as [8]

$$u_{i+1/2}^- = u_i^n + \frac{1+\eta}{4}(u_{i+1}^n - u_i^n) + \frac{1-\eta}{4}(u_i^n - u_{i-1}^n) \quad (2.9)$$

$$u_{i+1/2}^+ = u_{i+1}^n - \frac{1+\eta}{4}(u_{i+1}^n - u_i^n) + \frac{1-\eta}{4}(u_{i+2}^n - u_{i+1}^n) \quad (2.10)$$

The Essentially Non-Oscillatory schemes were first proposed by Harten, Osher, Engquist and Chakravarthy[12]. These schemes were developed to solve for flows containing both shocks and discontinuities as well as smooth regions. By using adaptive stencilling, a high order of accuracy is maintained right upto the discontinuity. For an  $r$ th order interpolation at a point, there are  $r$  available stencils. The one which yields the minimum absolute value of slopes and curvatures is chosen for the reconstruction. Stencils containing discontinuities are avoided, thus suppressing spurious oscillations. As an illustration, consider the piece-wise linear reconstruction given by equation (2.7). At point  $i$ , the slope  $S_i^n$  can be expressed as either  $u[x_i, x_{i+1}]$  or  $u[x_{i-1}, x_i]$ . The one which has a lower absolute value is chosen for the interpolation. Similarly, the coefficients for higher order terms are selected. At the boundaries, the number of candidate stencils decrease and thus inaccuracies may be generated due to the inability to avoid discontinuities. Also, higher order need not necessarily result in better resolution. In a solution field with more than one discontinuity in the neighborhood of each other, a higher order method would use a wider stencil and thus may not be able to avoid the discontinuous cells. In such a case, a lower order scheme with a narrower stencil would give better resolution. The algorithms used for implementing this technique can be found in [8, 12].

The original ENO schemes were based on constructing the dependent variable  $u(x, t)$  at the interfaces and then calculating the fluxes. This was modified by Shu and Osher [10, 11] and a number of ENO schemes were developed where the flux was directly calculated. Another modification was the shift from Lax-Wendroff type time-stepping to multi-stage Runge-Kutta time-stepping, as discussed in the next section. Some of these schemes are ENO-Roe, ENO-LF, ENO-LLF and ENO-RF [11]. They use the ENO stencilling with RP reconstruction. These schemes are more easily implemented for multi-dimensional problems and cases with non-zero source terms.

### 2.3.2 Time Evolution

Once the numerical flux function has been found, we obtain an ordinary differential equation (ODE), also called *semi-discrete* equation, of the form

$$\frac{du_i(t)}{dt} = -\frac{[\hat{g}_{i+1/2}^n - \hat{g}_{i-1/2}^n]}{\Delta x} \quad (2.11)$$

Several approaches have been adopted to solve this ODE. One of the approaches is to find the exact solution by integrating the fluxes in time from time level  $n$  to  $n+1$ , i.e,

$$u_i^{n+1} = u_i^n - \frac{1}{\Delta x} \int_{t^n}^{t^{n+1}} [\hat{g}_{i+1/2}^n - \hat{g}_{i-1/2}^n] dt \quad (2.12)$$

Some of the schemes using exact time evolutions are the MUSCL schemes developed by Van Leer and the Harten-Osher UNO schemes[8]. Another approach is the Lax-wendroff type time-stepping which involves approximating  $u^{n+1}$  in terms of  $u^n$  using a Taylor's expansion of the desired order and replacing the time derivatives by space derivatives. The Taylor expansion can be written as

$$u_i^{n+1} = u_i^n + u_t \Delta t + u_{tt} \frac{\Delta t^2}{2} + \dots \quad (2.13)$$

The time derivatives in the above expression are replaced by the space derivatives, based on the governing equation. For example, for the advection equation  $u_t + au_x = 0$ , the time derivatives can be replaced as  $u_t = -au_x$ ,  $u_{tt} = a^2 u_{xx}$ , etc. The spatial derivatives can be found from the spatial reconstruction used. This type of time-stepping was used by the ENO schemes proposed by Harten, Osher, Engquist and Chakravarthy [12]. The main disadvantage of this approach is in implementing this for multi-dimensional problems and problems with a source term. Replacement of time derivatives result in complicated expressions.

To overcome the difficulties in the Lax-Wendroff type time-stepping, the multi-stage Runge-Kutta (RK) ODE solver is used to solve equation (2.11). It is an improved version of the forward-Euler ODE solver. Equation (2.1) can also be expressed as

$$u_t = L(u) \quad (2.14)$$

The term  $L(u)$ . Let  $R(u)$  denote any  $r$ th order discrete approximation to  $L(u)$ , i.e,  $R(u) = L(u) + O(\Delta x^r)$ .  $R(u)$  is often called the *residue*. An  $m$ -stage RK time discretization is given as [11]:

$$u^{(i)} = u^{(0)} + \Delta t \sum_{k=0}^{i-1} c_{ik} R(u^{(k)}); i = 1, 2, \dots, m \quad (2.15)$$

with  $u^{(0)} = u^n$  and  $u^{n+1} = u^{(m)}$ . The behaviour of this scheme depends on the selection of the coefficients in the above equations.

## Chapter 3

### Maxwell's Equations

The theoretical concepts of electromagnetics are described by the basic laws formulated by Faraday, Ampere, Gauss, etc. They are combined into a set of vector equations to form the Maxwell's equations. These equations along with the equation for conservation of charge describe comprehensively the governing equations for any electromagnetic phenomenon. Also, they represent the unification of electric and magnetic fields. [13, 14]

These equations describe the relations between the source fields (current and charge distributions) and the mediating fields which are the electric and magnetic fields. The source fields are independent of the mediating fields and are related through the law of conservation of charge. These field equations describe both the spatial and temporal behavior of the fields. Along with these, there are a set of constitutive relations which describe the effect of the supporting medium on the fields.

The conservation of charge, also called the continuity equation, is given in the differential form as

$$\frac{\partial \rho}{\partial t} + \nabla \cdot \mathbf{J} = 0 \quad (3.1)$$

and in the integral form as

$$\int_V \frac{\partial \rho}{\partial t} dV + \int_{\partial V} \mathbf{J} \cdot d\mathbf{S} = 0 \quad (3.2)$$

Here,  $\rho$  is the charge density ( $C/m^3$ ) and  $\mathbf{J}$  is the current density ( $A/m^2$ ). Generally, the current density is the sum of impressed current density and the conduction current density,  $\mathbf{J} = \mathbf{J}_i$  (*impressed current*) +  $\mathbf{J}_c$  (*conduction current*). The conduction current is a function of the applied field as elaborated later.

#### 3.1 Differential form

The point form or the differential form is used to describe the fields relations at a single point at some instant of time. It is assumed that the field vectors are bounded and continuous functions of position and time and their derivatives exist and are continuous. Such points, where these conditions are satisfied are called *ordinary points* [14]. Discontinuities occur usually at material

interfaces, where there are differences in the electric and magnetic properties of the media and these are treated by the application of boundary conditions as described in later sections.

The differential form can be expressed as the following equations, also known as the Maxwell-Minkowski form [14, 15],

$$\frac{\partial \mathbf{B}}{\partial t} + \nabla \times \mathbf{E} = 0 \quad (3.3)$$

$$\frac{\partial \mathbf{D}}{\partial t} - \nabla \times \mathbf{H} + \mathbf{J} = 0 \quad (3.4)$$

$$\nabla \cdot \mathbf{D} = \rho \quad (3.5)$$

$$\nabla \cdot \mathbf{B} = 0 \quad (3.6)$$

The definitions and unit of each field variable are

- $\mathbf{E}$  - Electric field intensity ( $\text{V/m}$ )
- $\mathbf{H}$  - Magnetic field intensity ( $\text{A/m}$ )
- $\mathbf{D}$  - Electric flux density ( $\text{C/m}^2$ )
- $\mathbf{B}$  - Magnetic flux density ( $\text{W/m}^2$ )

The two divergence equations can be derived from the two curl equations if certain initial conditions are specified [14, 15]. Thus these equations are called *auxiliary equations*, providing initial values to the curl equations, called as *fundamental equations*.

### 3.2 Integral Form

The integral form of the Maxwell's equations are used to describe the relations between sources and the resulting fields over an extended, finite region of space. The field variables and their derivatives need not be continuous. This form can be derived from the differential form by integrating over a control volume and applying the Divergence and Circulation-Curl Theorems. The resultant equations are given as [13, 15]:

$$\iiint \frac{\partial \mathbf{B}}{\partial t} dV + \iint \hat{\mathbf{n}} \times \mathbf{E} dS = 0 \quad (3.7)$$

$$\iiint \frac{\partial \mathbf{D}}{\partial t} dV - \iint \hat{\mathbf{n}} \times \mathbf{H} dS + \iint \mathbf{J} dV = 0 \quad (3.8)$$

$$\iint \hat{\mathbf{n}} \cdot \mathbf{D} dS = \iint \rho dV \quad (3.9)$$

$$\iint \hat{\mathbf{n}} \cdot \mathbf{B} dS = 0 \quad (3.10)$$

### 3.3 Time Harmonic Fields and Wave Equation

In many practical situations, the fields encountered vary sinusoidally with time and are called as *time-harmonic fields*. Such variations can be expressed by relating the instantaneous fields to their complex phasor forms. A general field variable  $F$  can be expressed as  $F(x, y, z; t) = Re[F(x, y, z)e^{j\omega t}]$  where  $F$  represents the instantaneous value and  $\mathbf{F}$  represents the corresponding complex spatial form which are functions of position only. Time variation is given by the  $e^{j\omega t}$  term. In this form the time derivatives in the above equations can be replaced by multiplication by a factor of  $j\omega$ .

The Maxwell's equations can also be expressed as two second-order wave equations. These equations are in terms of electric or magnetic fields only and are thus decoupled. They can be alternatively used as the governing equations to solve a given problem. For time harmonic fields, the wave equations for a lossy media are given as follows [13]:

$$\nabla^2 \mathbf{E} = j\omega\mu\sigma\mathbf{E} - \omega^2\mu\epsilon\mathbf{E} \quad (3.11)$$

$$\nabla^2 \mathbf{H} = j\omega\mu\sigma\mathbf{H} - \omega^2\mu\epsilon\mathbf{H} \quad (3.12)$$

The conductivity of the media  $\sigma$  provides the loss mechanism (discussed in later sections). The wave equations for a non-lossy medium can be obtained by setting  $\sigma$  as zero and are of the form

$$\nabla^2 \mathbf{E} = -\omega^2\mu\epsilon\mathbf{E} = -\beta^2\mathbf{E} \quad (3.13)$$

$$\nabla^2 \mathbf{H} = -\omega^2\mu\epsilon\mathbf{H} = -\beta^2\mathbf{H} \quad (3.14)$$

The solution to these equations consist of positive and negative travelling waves with a propagation speed of  $c = 1/\sqrt{\mu\epsilon}$ .

### 3.4 Boundary Conditions

The differential form of the Maxwell's equations can be applied at ordinary points, i.e, where the fields are bounded and are continuous, as well as their derivatives exist and are continuous. Along the boundaries of the medium, discontinuities occur due to an abrupt change in material properties and these have to be treated by specifying necessary boundary conditions at the interfaces. At these interfaces, the derivatives of field variables are indeterminate and thus the point form of the Maxwell's equations cannot be used. The integral formulation has the advantage that propagation through various media can be treated by a single formulation by using the appropriate set of constitutive relations.

### 3.4.1 Finite Conductivity Media

The interface between two media characterized by  $(\epsilon_1, \mu_1, \sigma_1)$  and  $(\epsilon_2, \mu_2, \sigma_2)$  is considered. The boundary conditions can be derived by applying the integral form of the Maxwell's equations and the continuity equation on an infinitesimally small sub-domain straddling the interface. These can be summarized as follows [14]:

$$\hat{n} \times (\mathbf{H}_1 - \mathbf{H}_2) = \mathbf{J}_s \quad (3.15)$$

$$\hat{n} \times (\mathbf{E}_1 - \mathbf{E}_2) = 0 \quad (3.16)$$

$$\hat{n} \cdot (\mathbf{D}_1 - \mathbf{D}_2) = \rho_s \quad (3.17)$$

$$\hat{n} \cdot (\mathbf{B}_1 - \mathbf{B}_2) = 0 \quad (3.18)$$

$$\hat{n} \cdot (\mathbf{J}_1 - \mathbf{J}_2) = -\nabla \cdot \mathbf{J}_s - \frac{\partial \rho}{\partial t} \quad (3.19)$$

$\rho_s$  and  $\mathbf{J}_s$  are the impressed surface charge and current densities at the interfaces. In the absence of any such sources, the boundary conditions can be obtained by replacing them with zero.

### 3.4.2 Infinite Conductivity Media

At the surface of a perfect electric conductor (PEC), the tangential component of the electric field is zero because the free surface charges orient themselves so as to balance out the tangential component of the incident field. The boundary conditions can be expressed as [14]:

$$\hat{n} \times \mathbf{H} = \mathbf{J}_s \quad (3.20)$$

$$\hat{n} \times \mathbf{E} = 0 \quad (3.21)$$

$$\hat{n} \cdot \mathbf{D} = \rho_s \quad (3.22)$$

$$\hat{n} \cdot \mathbf{B} = 0 \quad (3.23)$$

$$\hat{n} \cdot \mathbf{J} = -\nabla \cdot \mathbf{J}_s - \frac{\partial \rho}{\partial t} \quad (3.24)$$

The fields inside the PEC are zero and these expressions describe the field values just outside the PEC surface.

### 3.5 Material Properties and Constitutive Relations

Electric and magnetic properties of the medium affect the electromagnetic fields existing inside that medium. On a macroscopic scale, this effect can be expressed by the constitutive relations, relating the flux density to the field intensity. For the electric field, this is given by

$$\mathbf{D} = \epsilon \mathbf{E} \quad (3.25)$$

where  $\epsilon$  is the permittivity of the medium. In free space (vacuum),  $\epsilon = \epsilon_0 = 8.854 \times 10^{-12}$  (farads/m). The relation between magnetic flux density and magnetic field intensity is similarly given by

$$\mathbf{B} = \mu \mathbf{H} \quad (3.26)$$

where  $\mu$  is the permeability of the medium. In free space,  $\mu = \mu_0 = 4\pi \times 10^{-7}$  (henries/m). The conduction current density,  $\mathbf{J}_c$  is related to the applied electric field as

$$\mathbf{J}_c = \sigma \mathbf{E} \quad (3.27)$$

In free space,  $\sigma = 0$ . However, inside a dielectric with finite conductivity, the current density is a sum of the impressed and conduction currents.  $\epsilon$ ,  $\mu$  and  $\sigma$  are known as *constitutive parameters* and their behavior depends on the material. In general, they are a function of the applied field strength, position, direction of applied fields and the frequency. On the basis of the behavior of the constitutive parameters, materials can be briefly classified as follows:

- A material is termed *linear* if the constitutive parameters do not vary with the strength of the applied field; otherwise it is non-linear.
- A material is called *homogenous* if the parameters do not vary with the position; else it is non-homogenous.
- A material is *isotropic* if these parameters are not a function of the direction of the applied fields; else it is anisotropic.
- A material is termed *dispersive* if these parameters do not vary with the frequency of the applied fields, else it is non-dispersive.

#### 3.5.1 Lossy Media

Equations (3.25) through (3.27) describe the macroscopic behavior of the fields propagating in the medium. On a microscopic level, the interaction between the fields and the medium

causes a polarization of the matter, due to the presence of charged particles inside the medium. There is a tendency of these particles to align themselves with the impressed fields, thus causing electric and magnetic polarization of the medium. The susceptibilities of the medium are given  $\chi_e$  (electric) and  $\chi_m$  (magnetic) [16]. The polarization vectors are denoted by  $\mathbf{P}$  and  $\mathbf{M}$  and are related to the applied fields as

$$\mathbf{P} = \epsilon_0 \chi_e \mathbf{E} \quad (3.28)$$

$$\mathbf{M} = \mu_0 \chi_m \mathbf{H} \quad (3.29)$$

The total flux inside the medium is the sum of the flux due to the applied field and the field due to polarization. This can be expressed as

$$\mathbf{D} = \epsilon_0 \mathbf{E} + \mathbf{P} \quad (3.30)$$

$$\mathbf{B} = \mu_0 \mathbf{H} + \mathbf{M} \quad (3.31)$$

The relation between the constitutive parameters inside the medium and those in free space can thus be expressed as

$$\epsilon = \epsilon_0 (1 + \chi_e) \quad (3.32)$$

$$\mu = \mu_0 (1 + \chi_m) \quad (3.33)$$

In a lossy dielectric, for a time-varying applied field, there is a finite time lag between the applied field and the polarization. Using frequency-domain expressions for representing harmonic fields, the permittivity and the permeability of the medium can be expressed as complex quantities[13, 16].

$$\epsilon = \epsilon' + j\epsilon'' \quad (3.34)$$

$$\mu = \mu' + j\mu'' \quad (3.35)$$

The imaginary parts of the above parameters depend on the time lag.

Applying these expressions to the Maxwell's curl equations for time-harmonic fields, we get the general form of the Maxwell's curl equations in a lossy medium as

$$\frac{\partial \mathbf{B}}{\partial t} = -\nabla \times \mathbf{E} - \rho \mathbf{H} \quad (3.36)$$

$$\frac{\partial \mathbf{D}}{\partial t} = \nabla \times \mathbf{H} - \mathbf{J}_i - \sigma \mathbf{E} \quad (3.37)$$

Here the loss mechanisms are provided by  $\rho = \omega \mu''$  (called as magnetic resistivity) and  $\sigma = \omega \epsilon'' + \sigma_s$  (called electric conductivity).  $\sigma_s$  is called the static field conductivity and  $\omega \epsilon''$  is the alternating field conductivity [13]. The sum is the equivalent conductivity of the medium. The loss tangents of the medium are defined as  $\tan \delta_e = \frac{\sigma}{\omega \epsilon'}$ ,  $\tan \delta_m = \frac{\rho}{\omega \mu'}$ , and are a measure of the lag between the polarization and applied fields.

### 3.5.2 Non-Lossy Media

For a non-lossy dielectric, the alternating field electric and magnetic conductivities of the medium are zero and thus the imaginary parts of the permittivity and permeability are zero. There is no time lag between the polarization and applied fields. Under these conditions, wave propagation in a non-lossy media are governed by

$$\frac{\partial \mathbf{B}}{\partial t} = -\nabla \times \mathbf{E} \quad (3.38)$$

$$\frac{\partial \mathbf{D}}{\partial t} = \nabla \times \mathbf{H} - \mathbf{J}_i - \mathbf{J}_c \quad (3.39)$$

The conduction current  $\mathbf{J}_c$  is purely due to the static field conductivity  $\sigma_s$  ( $\mathbf{J}_c = \sigma_s \mathbf{E}$ ). For the case of a perfect dielectric,  $\sigma_s = 0$  resulting in no conduction currents existing inside the medium, and therefore the current density is same as the impressed current density.

## Chapter 4

### Numerical Formulation and Solutions

To solve for the electromagnetic fields in time domain the Maxwell's curl equations are considered. For propagation in a non-lossy media, equations (3.38) and (3.39) are considered. In free space, the current density terms are absent thus giving a system of equations with no source terms. For propagation in a lossy medium, equations (3.36) and (3.37) are used.

To obtain the finite volume formulation for these equations, they are written in the conservation form as [5]

$$\mathbf{u}_t + f(\mathbf{u})_x + g(\mathbf{u})_y + h(\mathbf{u})_z = \mathbf{s} \quad (4.1)$$

where

$$u = \begin{bmatrix} B_x \\ B_y \\ B_z \\ D_x \\ D_y \\ D_z \end{bmatrix}, \quad f = \begin{bmatrix} 0 \\ -D_z/\epsilon \\ D_y/\epsilon \\ 0 \\ B_z/\mu \\ -B_y/\mu \end{bmatrix}, \quad g = \begin{bmatrix} D_z/\epsilon \\ 0 \\ -D_x/\epsilon \\ -B_z/\mu \\ 0 \\ B_x/\mu \end{bmatrix}, \quad h = \begin{bmatrix} -D_y/\epsilon \\ D_x/\epsilon \\ 0 \\ B_y/\mu \\ -B_x/\mu \\ 0 \end{bmatrix}, \quad s = \begin{bmatrix} -\rho H_x \\ -\rho H_y \\ -\rho H_z \\ -J_{ix} - \sigma E_x \\ -J_{iy} - \sigma E_y \\ J_{iz} - \sigma E_z \end{bmatrix}$$

This form can be derived from equations (3.36) and (3.37) by expanding the curl terms and separating the  $x$ ,  $y$  and  $z$  components. The corresponding equations for propagation in non-lossy medium and in free space can be obtained by replacing the lossy terms and source terms as zero respectively. The flux terms are homogenous of order one and thus the above equation can be written as

$$\mathbf{u}_t + A\mathbf{u}_x + B\mathbf{u}_y + C\mathbf{u}_z = \mathbf{s} \quad (4.2)$$

where  $A = f'(\mathbf{u})$ ,  $B = g'(\mathbf{u})$ ,  $C = h'(\mathbf{u})$  are the flux Jacobian matrices containing terms dependent on the constitutive parameters only [1]. In free space, the source term  $\mathbf{s}$  vanishes, giving

$$\mathbf{u}_t + A\mathbf{u}_x + B\mathbf{u}_y + C\mathbf{u}_z = 0 \quad (4.3)$$

The matrices  $A$ ,  $B$  and  $C$  are diagonalizable. The eigenvalues are

$$\{0, 0, 1/\sqrt{\mu\epsilon}, 1/\sqrt{\mu\epsilon}, -1/\sqrt{\mu\epsilon}, -1/\sqrt{\mu\epsilon}\}$$

Although the eigenvalues are repeated, it is possible to find a complete set of eigenvectors and thus the system is hyperbolic [1]. The integral form equation (4.1) is the basis for all FVTD schemes and is expressed as

$$\int_{D_i} \frac{\partial \mathbf{u}_i}{\partial t} dV + \int_{\partial V_i} \mathbf{F} \cdot d\mathbf{s} = \int_{V_i} \mathbf{s} dV \quad (4.4)$$

where the flux tensor  $\mathbf{F} = f(\mathbf{u})\hat{i} + g(\mathbf{u})\hat{j} + h(\mathbf{u})\hat{k}$ .

#### 4.1 Characteristic based algorithms

The Maxwell's equations in conservation form constitute a hyperbolic system of PDEs. Thus characteristic-based algorithms are particularly useful for solving these equations. These algorithms aim to achieve the approximate Riemann formulation by diagonalizing the coefficient matrices in each spatial direction at a time. The fluxes at the cell interfaces are split into their positive and negative travelling contributions, according to the sign of the eigenvalues and stencils used for reconstruction are biased in the direction opposite to that of the wave propagation (upwind). This windward discretization imitates the physical propagation of waves and is more stable than central differencing. High resolution schemes with directionally biased stencils have been observed to give good results.

One example of such a scheme is developed in [1] where propagation in a non-lossy media has been considered. The governing equations (equation (4.2)) is discretized as

$$\frac{\Delta U}{\Delta t} + \frac{\Delta(AU)}{\Delta x} + \frac{\Delta(BU)}{\Delta y} + \frac{\Delta(CU)}{\Delta z} - J = 0 \quad (4.5)$$

Here,  $x$ ,  $y$  and  $z$  are the locally orthogonal coordinates for a cell. The flux is split along these coordinates and  $\Delta x$ ,  $\Delta y$  and  $\Delta z$  are based on the shape and size of the cell. In such a scheme, the stretching ratio between volumes of adjacent cells affects the accuracy, since an averaged behavior has been assumed inside the cell. The fluxes at the interfaces are reconstructed using the Anderson-Thomas-Van Leer upwind based reconstruction. The flux at the interface is split as

$$(AU)_{i+1/2} = (AU)_{i+1/2}^+ + (AU)_{i+1/2}^- \quad (4.6)$$

and similarly for the other fluxes. The variable at the interface  $U_{i+1/2}^+$  and  $U_{i+1/2}^-$  are reconstructed using equations (2.11) and (2.12). Using a similar approach, a third order upwind based scheme has also been developed in [1].

Another characteristic-based algorithm, developed in [5, 6] uses the ENO concept. The algorithm is required to solve for scattering by the PEC surface coated with a dielectric (lossy/non-lossy). The discontinuity at the free-space dielectric interface makes a non-oscillatory algorithm

attractive. The scattered formulation is used which provides a unified framework within which propagation can be solved in both free space and dielectric. For grid cells containing the dielectric, the appropriate source term is added. Thus the need for impedance boundary conditions is dispensed with. Due to the linearity of Maxwell's equations, equation (4.1) can be split into the incident and scattered field. The semi-discrete equation using the scattered formulation is

$$\left(\frac{\partial \mathbf{u}_i^{sca}}{\partial t}\right)V_i + \sum_{m=1}^M [(\mathbf{F}(\mathbf{u}^{inc}) + \mathbf{F}(\mathbf{u}^{sca})).\hat{\mathbf{n}}S]_i = (\mathbf{s}_i^{inc} + \mathbf{s}_i^{sca} - \frac{\partial \mathbf{u}_i^{inc}}{\partial t})V_i \quad (4.7)$$

The terms involving the incident field  $\mathbf{u}^{inc}$  can be evaluated analytically. The scattered source term  $\mathbf{s}^{sca}$  is evaluated based on the cell-centered values of  $\mathbf{u}^{sca}$  at the beginning of the time-step. The flux due to scattered field  $\mathbf{F}(\mathbf{u}^{sca})$  is evaluated using the ENO-Roe algorithm [11]. The algorithm constructs the flux directly by selecting the stencil according to the ENO technique. The initial point selected in the iterative algorithm involved in stencil selection and reconstruction may lie on either side of the interface and this is decided by the sign of the *Roe speed*, which introduces an upwind nature into the flux reconstruction. The result is an ODE which is solved by two stage Runge-Kutta time-stepping.

## 4.2 Dual Grid approach

In [4], an algorithm based on dual grid has been developed and demonstrated. All electric field components lie on the same grid point while the magnetic field components lie on the corresponding dual grid point. The dual grid points are constructed by taking the average of the coordinates of the corners of each grid cell. This imitates the physics of the Maxwell's curl equations, since a time-varying magnetic field has an electric field curling around it and vice versa. Here a typical cell consists of an H-field at the center with E-fields at the corners. The value of the H-field at the center is updated using the fluxes due to the E-field values at the corners, i.e, the circulation of the electric field along the cell boundaries and vice-versa. Time stepping is through a four stage RK method. Two RK time-evolution are carried out, one updating the electric fields at the grid points and the other updating the magnetic fields at the dual grid points.

## 4.3 Numerical Boundary Treatment

### 4.3.1 Surface Boundary Conditions

Typically, FVTD algorithms are used to compute the electric field propagation through various media and scattering by some object. Thus the surface boundary consists of a PEC surface. At

this surface, the physical boundary conditions dictate zero tangential component of the electric field, i.e.,

$$\hat{n} \times \mathbf{E} = 0 \quad (4.8)$$

Thus any numerical boundary treatment has to explicitly set the tangential electric field to zero at the near field boundary. In the scattered field formulation, this condition is implemented on the surface of the body as

$$\hat{n} \times \mathbf{E}^{sca} = -\hat{n} \times \mathbf{E}^{inc} \quad (4.9)$$

where the value of  $\mathbf{E}^{inc}$  can be found analytically from the incident field expression. Similarly the physical boundary condition for the magnetic field requires that the normal component be zero at the PEC surface, i.e,

$$\hat{n} \cdot \mathbf{B} = 0 \quad (4.10)$$

The scheme should thus explicitly set the normal magnetic field to zero at the boundary. For the scattered field formulation, this is enforced on the surface of the body as

$$\hat{n} \cdot \mathbf{B}^{sca} = -\hat{n} \cdot \mathbf{B}^{inc} \quad (4.11)$$

In the ghost cells, the tangential electric fields for the ghost cells are extrapolated using the computed value of  $\hat{n} \times \mathbf{E}^{sca}$  at the surface of the scatterer and the cell centered values of the cells above the surface. The normal components are taken identical to those above the scatterer. Similarly, the magnetic field in the ghost cells is computed.

### 4.3.2 Far Field

The far-field boundary is an artificial boundary due to the truncation of the domain. This is necessary due to the finite size of the computer memory. The boundary treatment should be such that outgoing waves are allowed to exit the domain without any reflection. The incoming waves should also be specified since they carry the data from outside the domain (freestream). Incoming and outgoing data are carried along characteristics and thus specification of the characteristic variables by freestream values or values from inside the domain are the best option. Such far-field boundary treatment are called characteristic based boundary conditions. Specification of incoming characteristics as free-stream values is debatable since outgoing waves are a violation of the assumption that conditions at far field are same as freestream. For dissipative schemes, this factor is not overly critical since the outgoing waves get dissipated before reaching the far-field boundary.

To prevent reflection of outgoing waves, the non-reflecting or absorbing boundary conditions are used, which ensure that waves leave the domain cleanly. As an example, use of zero-order extrapolation for the outgoing characteristic for the ghost cells results in a Riemann problem at the boundary with zero jump. Thus no waves are generated. This kind of treatment is effective for plane waves exiting normal to the boundary but fails for other cases, causing loss of information [7]. A wave at an angle to the boundary can be resolved into parallel and perpendicular components. If any of these is an incoming wave, it gets cut out. For such cases, more complicated absorbing boundary conditions have to be designed.

Most FVTD algorithms in CEM use characteristic absorbing boundary conditions. The scattered field at the far field is decomposed along characteristics normal to cell faces. The incoming fluxes are set to zero. The direction of propagation of the wave is given by

$$[(\mathbf{E} \times \mathbf{H}) / |\mathbf{E} \times \mathbf{H}|] \quad (4.12)$$

and if the local coordinates of the cell are aligned in this direction, then wave reflection can be completely eliminated. In other cases, the undesirable reflections are considerably lesser [1, 5]. Recently, multi-dimensional characteristic-based absorbing boundary condition (MDC-ABC) has been developed for better suppression of spurious reflection [2]. Its performance has been demonstrated to be considerably better.

#### 4.4 An Application: RCS Computations

One of the problems where the FVTD framework has been used extensively is the computation of scattering by complex configurations, especially aircraft. Scattering is characterized by the electric size of the body which is defined as  $ka$  where  $k$  is the wave number ( $2\pi/\lambda$ ) of the incident radiation and  $a$  is any characteristic length of the body (say wingspan for an aircraft). One of the parameters quantifying the scattering by a body is its *Radar Cross-Section* (RCS), defined as the area of an isotropic reflector returning the same power per solid angle as the given body. At far field, it is proportional to the ratio of the power received from the target to the power incident on the target.

$$\sigma = \lim_{R \rightarrow 0} 4\pi R^2 \frac{I_r}{I_i} \quad (4.13)$$

where  $I_r$  is the power received per unit area of the receiver and  $I_i$  is the power intercepted per unit area by the target. The RCS is expressed in units of  $m^2$  or dBsm when normalized with  $1m^2$  or dB when normalized with the square of the wavelength.

The FVTD algorithm is used to compute the total fields in the the numerical domain from which the equivalent surface currents on the body of the scatterer can be calculated as [13]

$$\mathbf{J}_s = \hat{\mathbf{n}} \times \mathbf{H} \text{ (equivalent electric current)} \quad (4.14)$$

$$\mathbf{M}_s = -\hat{\mathbf{n}} \times \mathbf{E} \text{ (equivalent magnetic current)} \quad (4.15)$$

A far-field transform is used to calculate the scattered fields  $\mathbf{E}_{sc}$  and  $\mathbf{H}_{sc}$  at infinite distance from the scatterer due to these surface currents and the RCS is calculated as

$$\sigma = 4\pi R^2 \frac{|\mathbf{E}_{sc}|^2}{|\mathbf{E}_{inc}|^2} \quad (4.16)$$

where R is taken to be a sufficiently large number (for example, in [5, 6] R is taken as 100,000).

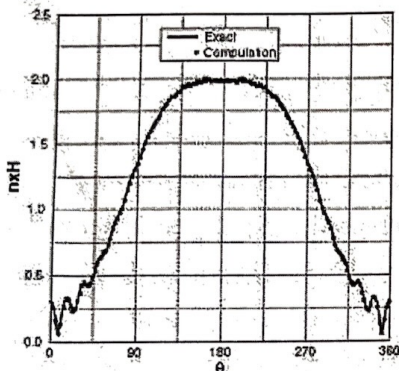


Figure 4.1: Surface currents (cylinder)

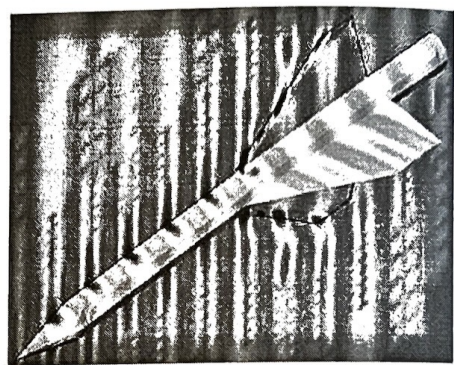


Figure 4.2: Computed  $H_z$  for a cruciform missile

at 72 MHz

Figure (4.1) shows the electric surface currents computed for a cylinder with a PEC surface [2]. Such canonical shapes are chosen for which analytical results exist for validation of the algorithm. The grid resolution chosen here is 20 points per wavelength at the surface, with the far field boundary located at  $2\lambda$  away. The CFL number chosen is 1. Figure (4.2) shows the computed z-component of the magnetic fields due to a cruciform missile with a PEC surface at 72 MHz [2]. The length of the body is  $11\lambda$  and the grid resolution used is 20 points per wavelength at the surface.

Figure (4.3) and (4.4) show results from [5] where an ENO-based algorithm has been used to compute the scattering. Figure (4.3) shows the RCS variation with the viewing angle in the equatorial plane for a sphere coated with non-lossy discontinuous coating. The electric size considered here is 2.6858 while the thickness of the dielectric coating is  $0.05\lambda$ . Figure (4.4)

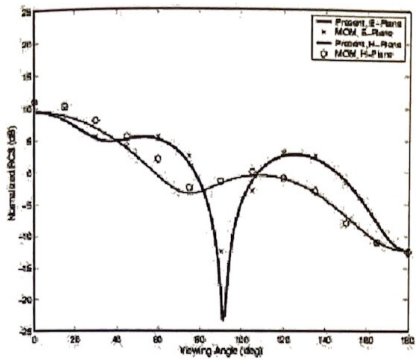


Figure 4.3: RCS of a sphere

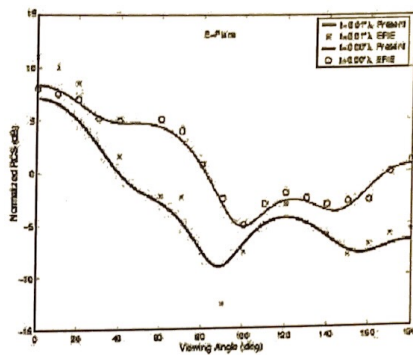


Figure 4.4: RCS of a Cone-sphere

shows RCS variation with the viewing angle of a cone sphere with vertex angle of 90 degrees and sphere diameter  $0.955\lambda$  covered with a lossy dielectric.

Figures (4.5) and (4.6) are the RCS computed for some canonical low-observable shapes [4]. The ogive and the NASA almond are Electromagnetic Code Consortium (EMCC) benchmarks [4, 17]. To reduce the RCS, the nose of an aircraft is often shaped like an ogive. In figure (4.5), the ogive is a PEC with a half angle of 22.62 degrees, an aspect ratio of 5:1 and length of 10 inches. The variation of backscatter RCS with the frequency upto 5 GHz is plotted. The resolution at 5 GHz was 20 cells per wavelength. Figure (4.6) show the monostatic RCS variation of the almond when illuminated from angles ranging from 0 to 180 degrees at steps of 15 degrees at 1.19 GHz. Experimental data has been used to validate the numerical results.

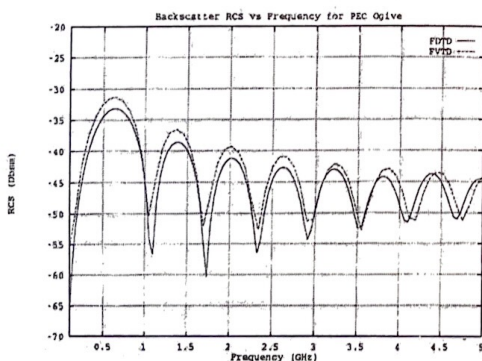


Figure 4.5: RCS of an ogive

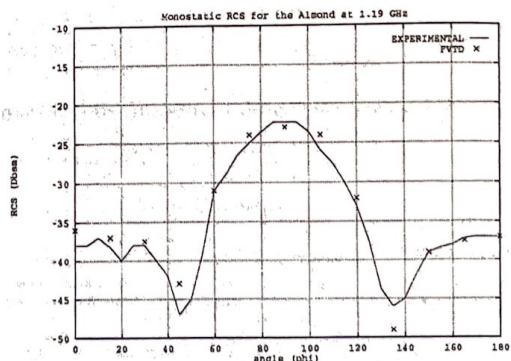


Figure 4.6: RCS of a NASA almond

Figure (4.7) show the RCS variation for a clean delta wing configuration [6]. Such planforms are expected to have a low RCS and thus can be called as a low-observable configration. The

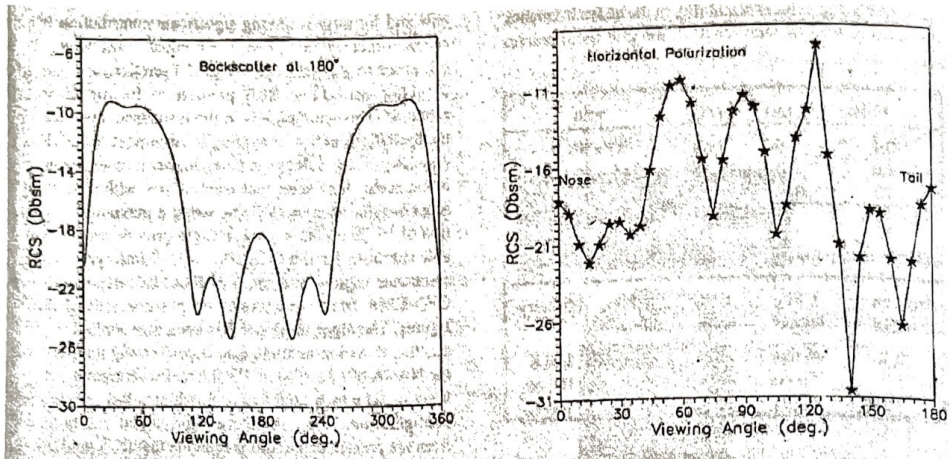


Figure 4.7: RCS for a clean delta wing

body has been assumed to be a PEC. The computations are carried out at an electric size of 1.7, corresponding to a frequency of 54 MHz with a horizontal polarization. The left-hand side graph shows the variation of the bistatic RCS in the yaw plane at nose-on incidence while the right-hand side graph shows the variation of monostatic RCS at various angle of incidence in the yaw plane.

There is lack in existing literature of RCS computation for actual aircraft, especially low-observable (stealthy) configurations. In [1], a 3rd order finite volume code has been used to compute the scattered fields by the re-entry vehicle X24C-10D, illuminated by a transverse electric excitation. The electric size is around 9.3 and a grid resolution of atleast 18 cells per wavelength has been used. However the results are unvalidated.

## Chapter 5

### Conclusions

The development of the FVTD framework and its application to problems in electromagnetism has considerably simplified the process of obtaining solution of the Maxwell's equations, especially for complicated geometries. One of the major applications of the FVTD schemes is computing the scattering from bodies. Analytical solutions and numerical methods like sum-of-components are restricted in scope. In such cases the FVTD framework provides an ideal solution scheme. For complicated geometries, the FVTD scores over FDTD with its ability to handle body-conformal grids without the need for grid transformation.

Numerical results indicate that characteristic based algorithms are very effective in solving the Maxwell's equations due to their hyperbolic nature. Validation of results with analytical ones for canonical shapes usually result in excellent agreement. However, one of the major drawbacks of the FVTD algorithms is the huge computational requirement. Computations for practical problems, for example, scattering from an aircraft, require a huge memory as well as fast processor speeds. Recent FVTD algorithms are designed for parallel platforms. Although parallelization issues have been excluded from this study, it should be noted that solutions through serial codes take impractically long time. Computations for scattering and RCS for aircrafts is presently restricted to below 1 GHz. One of the aims of recent efforts is the prediction of RCS of aircraft in the X-band (around 10 GHz).

Another drawback is the lack of literature on the optimum grid resolutions required for computation of solutions. Presently, estimates are empirical and based on numerical experiments. For calculating the fields at a particular wavelength, the Nyquist sampling theorem specifies a minimum fineness of the grid as at least two grid cells per wavelength. The fineness of the grid has been observed to affect the time required for the solution to converge. A measure of the minimum distance to the far-field boundary based on theory is also absent. Numerical experiments [6] found it to be dependent on the wavelength at low electric sizes and the body dimensions at higher electric sizes.

Inspite of these drawbacks, the FVTD scheme has been found to be a viable alternative to other methods. Also, it has the potential to compute solutions which may not be possible using methods based on analytical theories.

# References

1. J.S. Shang, *Characteristic-based Algorithms for Solving Maxwell's Equations in Time Domain*, IEEE Trans. Antennas Propagation, Vol. 37, No. 3, 1995
2. Z.J. Wang, et al, *A FV-TD electromagnetic solver using adaptive Cartesian grids*, Computer Physics Communication, Vol. 148, 2002
3. A Sommerfield, *Partial Differential Equations in Physics*, Academic Press, New York, 1949
4. V. Ahuja and L.N. Long, *A parallel finite-volume Runge-Kutta algorithm for electromagnetic scattering*, Journal of Computational Physics, Vol. 137, No. 2, 1997
5. A. Chatterjee and A. Shrimal, *Essentially Non-Oscillatory finite volume scheme for electromagnetic scattering by thin dielectric coatings*, AIAA Journal - to appear
6. A. Chatterjee and S.P. Koruthu, *Characteristic based FVTD scheme for predicting electromagnetic scattering by aerospace configurations*, Journal of The Aeronautical Society of India, Vol. 52, No. 3, 2000
7. R.J. Leveque, *Finite Volume Methods for Hyperbolic Problems*, Cambridge University Press, Cambridge, 2002
8. C. Laney, *Computational Gasdynamics*, Cambridge University Press, Cambridge, 1998
9. Ronghua, et al, *Generalized difference methods for differential equations: numerical analysis of finite volume methods*, Marcel Dekker, New York, 2000
10. C.W. Shu and S. Osher, *Efficient implementation of essentially non-oscillatory shock capturing schemes*, Journal of Computational Physics, Vol. 77, No. 2, 1988
11. C.W. Shu and S. Osher, *Efficient implementation of essentially non-oscillatory shock capturing schemes II*, Journal of Computational Physics, Vol. 83, No. 1, 1989
12. A. Harten, B. Engquist, S. Osher and S. Chakravarthy, *Uniformly high-order accurate essentially non-oscillatory schemes III*, Journal of Computational Physics, Vol. 71, No. 2, 1987
13. C.A. Balanis, *Advanced Engineering Electromagnetics*, John Wiley, New York, 1989
14. E. Rothwell and M. Cloud, *Electromagnetics*, Boca Raton, CRC Press, 2001
15. J.A. Kong, *Electromagnetic Wave Theory*, John Wiley, New York, 1986
16. R.M. Jha, et al, *Radar Absorbing Materials: from theory to design and characterization*, Kluwer Academic Pub., Boston, 1996
17. A.C. Woo, H.T.G. Wang, M.J. Schuh and M.L. Sanders, *EM programmer's notebook-benchmark radar targets for the validation of computational electromagnetics programs*, IEEE Antennas and Propagation Magazine, Vol. 35, No. 1, 1993

# Acknowledgements

I would like to express my sincere gratitude towards my guide, Prof. Avijit Chatterjee, for his invaluable guidance and constant encouragement throughout the course of this seminar, without which this study would not have been possible. I would also like to acknowledge the help I have received from Research Assistant Manoj B. Vaghela who shared his considerable practical experience in this field with me.

*Debojyoti*

Debojyoti Ghosh